JOC The Journal of Organic Chemistry

pubs.acs.org/joc Note

# How the Lewis Base $F^-$ Catalyzes the 1,3-Dipolar Cycloaddition between Carbon Dioxide and Nitrilimines

Dennis Svatunek,[+] Thomas Hansen,[+] Kendall N. Houk, and Trevor A. Hamlin*

Cite This: J. Org. Chem. 2021, 86, 4320−4325 Read Online



**ABSTRACT:** The mechanism of the Lewis base $F^-$ catalyzed 1,3-dipolar cycloaddition between $CO_2$ and nitrilimines is interrogated using DFT calculations. $F^-$ activates the nitrilimine, not $CO_2$ as proposed in the literature, and imparts a significant rate enhancement for the cycloaddition. The origin of this catalysis is in the strength of the primary orbital interactions between the reactants. The Lewis base activated nitrilimine−$F^-$ has high-lying filled FMOs. The smaller FMO-LUMO gap promotes a rapid nucleophilic attack and overall cycloaddition with $CO_2$.

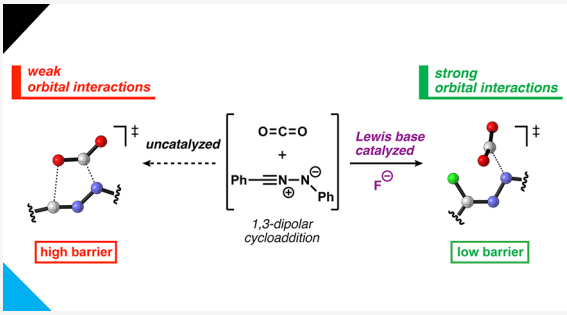




The general use of small, highly abundant organic molecules, such as carbon dioxide ($CO_2$), as building blocks in organic synthesis by activation and selective transformation to useful chemicals is highly attractive from both an economic and societal point of view.[1] Carbon dioxide is a desired feedstock for more complex hydrocarbon derivatives, since it is an abundant green-house gas that is cheap.[2] Chemists have engaged in significant efforts toward crafting methods to activate these otherwise unreactive molecules; however, it is in many cases a trial-and-error process, as the factors that play a role in the bond activation are not entirely understood.

In 2017, Lu and co-workers developed a convenient methodology to efficiently activate $CO_2$ by $F^-$ (used as CsF/18-crown-6) and subsequently trap it with nitrilimines via a 1,3-dipolar cycloaddition to access 1,3,4-oxadiazole-2(3*H*)-ones (Scheme 1).[3] In this reaction, $F^-$ first acts as a base to produce the nitrilimine intermediate (i.e., a 1,3-dipole) from hydrazonyl chloride. The nitrilimine then undergoes a cycloaddition reaction with $CO_2$ (i.e., dipolarophile) to form the oxadiazolone. It was found that the presence of a base (e.g., amines or carbonates) alone does not facilitate efficient conversion to the product, but instead generates a large amount of the (undesired) dimerized dipole product.

**Scheme 1. Proposed Mechanism of the Fluoride-Catalyzed 1,3-Dipolar Cycloaddition between $CO_2$ and Nitrilimines by Lu and Co-workers, in Which the Lewis Base $F^-$ Together with $CO_2$ Forms the Activated Dipolarophile (i.e., $CO_2F^-$);[3] $R^1$ and $R^2$ = Aryl or Alkyl**

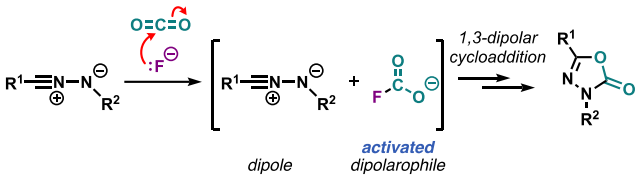


The authors proposed the formation of the known and stable fluorocarbonate ($CO_2F^-$),[4] formed from $CO_2$ and $F^-$. Fluorocarbonate has been suggested to enhance the reactivity of $CO_2$ in some reactions (Scheme 1).[5] The use of simple Lewis bases (e.g., $F^-$) as catalysts for the activation of small molecules, which allows for efficient transformations under mild conditions, is of high interest.[6] Merino and co-workers previously investigated this reaction computationally and provided evidence for an operative mechanism based on the analysis of a number of possibly competing potential energy surfaces; however, they did not comment on the origin of the catalytic effect of the $F^-$ Lewis base.[7] Lu and co-workers experimentally showed that a base alone does not efficiently facilitate the cycloaddition reaction, so that $F^-$ is playing another role, presumably as a catalyst.[3] In contrast to the work of Merino et al., this indicates that $F^-$ does not solely act as a base. It is widely accepted that these 1,3-dipoles are readily formed from the hydrazonyl chloride, even in the presence of weak bases.[8] We have revisited the mechanism of this formal 1,3-dipolar cycloaddition between $CO_2$ and nitrilimine to identify the catalytic role of the $F^-$ in this transformation.

Received: December 18, 2020
Published: February 12, 2021





https://dx.doi.org/10.1021/acs.joc.0c02963
J. Org. Chem. 2021, 86, 4320−4325

Three possible reaction pathways (Scheme 2) have been investigated, using state-of-the-art DFT calculations, to unravel the physical mechanism behind the Lewis base $F^-$ activation in 1,3-dipolar cycloaddition reactions: (i) the uncatalyzed cycloaddition, (ii) the activation of the dipolarophile, by the generation of $CO_2F^-$ by $F^-$, followed by the cycloaddition, and (iii) the activation of the dipole by the addition of $F^-$ to nitrilimine **1** forming activated nitrilimine−$F^-$ **2**, followed by the cycloaddition. In order to pinpoint the actual role of $F^-$ in lowering the reaction barrier, we selected the model system depicted in Scheme 2. We found that the inclusion of $Cs^+$ and 18-crown-6, as Merino and co-workers did, slightly raises the reaction barrier due to the fact that $F^-$ is less Lewis basic because of the interaction with the $Cs^+$ (Supporting Information Figure S1), while the overall mechanism remained unchanged.

**Scheme 2. Possible Reaction Pathways for the 1,3-Dipolar Cycloaddition between Carbon Dioxide and Nitrilimine 1 in the Presence of the Lewis Base $F^-$**

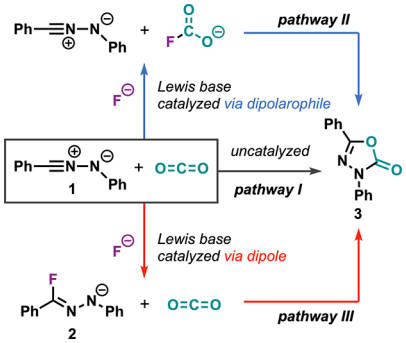


To identify the origin of the catalytic effect of the Lewis base, we employed the distortion/interaction−activation strain model[9] in combination with Kohn−Sham molecular orbital (KS-MO)[10] theory and energy decomposition analysis (EDA).[11] This methodological approach facilitates the analysis of the potential energy surface and, more importantly, the activation barrier, by decomposing the total energy of the system into chemically meaningful and easily interpretable terms and has been used by us to study other related 1,3-dipolar cycloadditions.[12]

The reaction profiles of the three reaction pathways of the studied 1,3-dipolar cycloaddition between carbon dioxide and nitrilimine **1** in the presence of the Lewis base $F^-$, as well as their key transition state structures, are shown in Figure 1. The uncatalyzed pathway (i.e., pathway I; black) follows a concerted cycloaddition reaction with a barrier of $\Delta G^{\ddagger}$ = 22.7 kcal $mol^{-1}$ leading to product **3** (Figure 1a). The transition state, I-TS, is highly asynchronous, but is still concerted, with a C···N distance of 1.57 Å and a C···O distance of 2.33 Å (Figure 1b). This relatively high computed reaction barrier is consistent with the experimentally observed dimerization of nitrilimine **1** in the absence of $F^-$, a process that goes with a more favorable barrier of $\Delta G^{\ddagger}$ = 20.1 kcal $mol^{-1}$ (see SI Figure S2).[3]

Pathway II (blue) begins with the exergonic ($\Delta G_{rxn}$ = −18.9 kcal $mol^{-1}$) formation of $CO_2F^-$ from $CO_2$ and $F^-$. Coodination of $F^-$ to $CO_2$ is driven by stabilizing covalent and electrostatic interactions and induces a buildup of electron density on the oxygens of $CO_2F^-$ compared to $CO_2$ (see SI Table S1 and Figure S3). This leads, in contrast to pathway I, to a stepwise mechanism, whereby addition of the oxygen of the $CO_2F^-$ to the electrophilic imine carbon center in II-TS occurs first and leads to II-INT (Figure 1b). This is the rate-limiting step of pathway II and goes with a reaction barrier of $\Delta G^{\ddagger}$ = 16.2 kcal $mol^{-1}$, which is 6.5 kcal $mol^{-1}$ lower than the uncatalyzed cycloaddition. Next, II-INT undergoes ring closure via a near barrierless pathway through II-TS2 ($\Delta G^{\ddagger}$ = 1.2 kcal $mol^{-1}$). Formation of product **3** and $F^-$ from II-INT2 is endergonic; however, the $F^-$ transfer, either to a second molecule of $CO_2$ leading to **3** and $CO_2F^-$ or to a second nitrilimine leading to **3** and **2**, is exergonic. Lastly, pathway III (red), which like pathway II proceeds via a stepwise process, first begins with the barrierless formation of a Lewis base (or nucleophilic catalyst) activated nitrilimine−$F^-$ (i.e., **2**) by the coordination of $F^-$ on the electrophilic nitrile carbon of nitrilimine **1** (see SI Figure S6). Formation of **2** is highly exergonic ($\Delta G_{rxn}$ = −34.2 kcal $mol^{-1}$) and is more than twice as favorable compared to the formation of $CO_2F^-$ due to even more stabilizing covalent and electrostatic interactions (pathway II; blue, $\Delta\Delta G_{rxn}$ = −15.3 kcal $mol^{-1}$; see Table S1). The imine nitrogen of nitrilimine−$F^-$ **2** exhibits an increased electron density, compared to dipole **1** (see SI Figure S3), and can engage in an efficient addition to $CO_2$. Activated

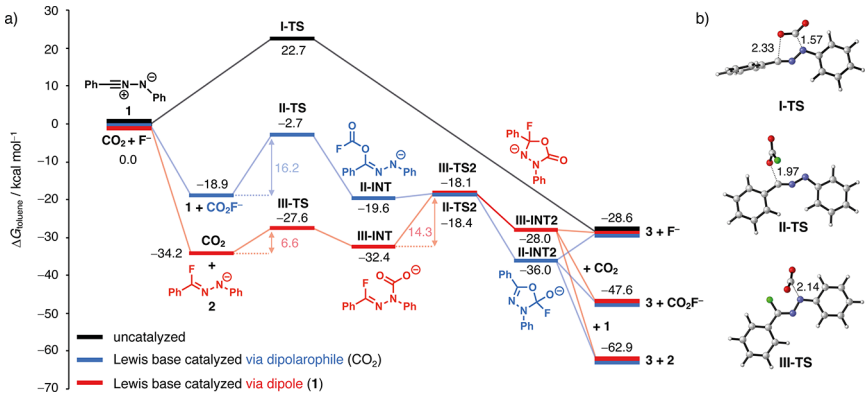


**Figure 1.** (a) Reaction profiles ($\Delta G_{toluene}$ in kcal $mol^{-1}$) for the three reaction pathways of the studied 1,3-dipolar cycloaddition between carbon dioxide and nitrilimine **1**, including (i) uncatalyzed cycloaddition (black), (ii) formation of $CO_2F^-$ followed by stepwise cycloaddition (blue), and (iii) formation of **2** followed by stepwise cycloaddition (red), computed at SMD(toluene)-M06-2X-D3/def2-TZVP; TS = transition state and INT = intermediate. (b) Key transition state structures with key bond lengths (in Å) for the three reaction pathways.


https://dx.doi.org/10.1021/acs.joc.0c02963
J. Org. Chem. 2021, 86, 4320−4325

nitrilimine−$F^-$ **2** can then proceed through transition state III-TS with a very low barrier of only 6.6 kcal $mol^{-1}$, resulting in III-INT. This intermediate then undergoes intramolecular ring formation, through III-TS2 with a barrier of 14.3 kcal $mol^{-1}$, to then form product **3** and regain the Lewis base $F^-$. We have also computed pathway III with the corresponding $Cl^-$ adduct of **1**, which is a similar intermediate to that proposed by Merino and co-workers,[7] and we found that $F^-$ adduct **2** follows a lower energy pathway in the reaction with $CO_2$ (see Supporting Information, Schemes S1−S3 and Figure S1).

In order to gain quantitative insight into the physical factors why Lewis base catalyzed (i.e., nucleophilic-catalyzed) reaction pathway III is highly favored over the uncatalyzed pathway I, we turned to the distortion/interaction−activation strain model (D/I-ASM).[9] The D/I-ASM decomposes the electronic energy ($\Delta E$) into two distinct energy terms, namely, the strain energy ($\Delta E_{strain}$) and the interaction energy ($\Delta E_{int}$). The strain energy results from the deformation of the individual reactants and the interaction energy accounts for all chemical interactions between the deformed reactants along the reaction coordinate, defined, in this case, as the forming N···C bond.[12] As previously discussed, pathway I goes with a reaction barrier of 22.7 kcal $mol^{-1}$, while the first step of pathway III proceeds with a barrier of only 6.6 kcal $mol^{-1}$. Figure 2a shows the D-I/ASM analysis of pathway I (black) and pathway III (red). The origin of the lower barrier, in terms of electronic energy (trends are consistent for $\Delta E^{\ddagger}$ and $\Delta G^{\ddagger}$) for Lewis base catalyzed pathway III, can be traced exclusively to a more stabilizing interaction energy, while having a comparable strain energy.

The interaction energy between the deformed reactants can be further analyzed in terms of quantitative Kohn−Sham molecular orbital theory (KS-MO)[10] together with a canonical energy decomposition analysis (EDA).[11] The EDA decomposes the $\Delta E_{int}$ into the following four physically meaningful energy terms: electrostatic interactions ($\Delta V_{elstat}$), (steric) Pauli repulsion ($\Delta E_{Pauli}$), orbital interactions ($\Delta E_{oi}$), and disperision interactions ($\Delta E_{disp}$). The EDA (Figure 2b) shows that the more stabilizing $\Delta E_{int}$ for the Lewis base catalyzed pathway III originates from a significantly more stabilizing $\Delta E_{oi}$. The $\Delta V_{elstat}$ is slightly more stabilizing and the $\Delta E_{Pauli}$ remains almost unchanged. The origin of the more stabilizing of the Lewis base catalyzed pathway can be analyzed and explained by means of a Kohn−Sham molecular orbital analysis (KS-MO). We have quantified the key occupied−unoccupied orbital interaction between the FMO of **1** and **2** and the antibonding unoccupied orbital of $CO_2$ at consistent geometries with a N···C bond length of 2.14 Å (Figure 2c). The stronger orbital interaction of the Lewis base catalyzed pathway could be traced back to the smaller FMO energy gap for the normal electron demand (NED) orbital interactions with the $LUMO_{CO2}$. This originates from the much higher energy of the filled FMOs of **2** (i.e., nitrilimine−$F^-$), compared to **1** (i.e., uncatalyzed pathway). The HOMO of **2** also shows a similar trend, but the overlap is much lower since the orientation of this orbital is nearly orthogonal to the $LUMO_{CO2}$ (see SI Figure S4). In all, the presence of the negatively charged Lewis base $F^-$ in **2** causes a significant negative external potential that destabilizes the FMOs (see SI Figure S5). Additionally, the FMOs, especially the HOMO−$1_2$, are further destabilized as a result of (steric) Pauli repulsion with the filled FMOs of $F^-$ (see SI Figure S5).

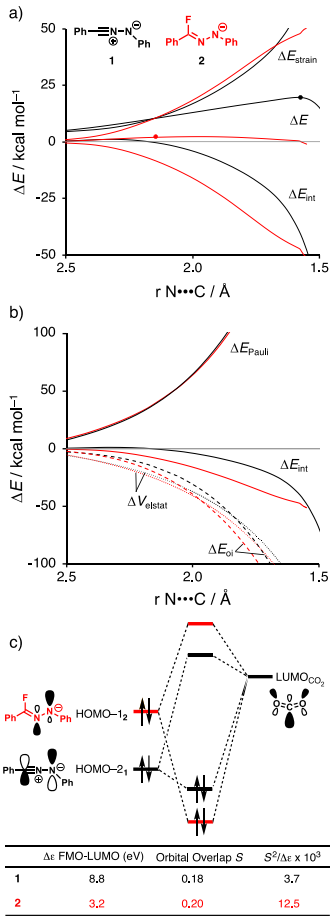


| | Δε FMO-LUMO (eV) | Orbital Overlap S | $S^2/\Delta\varepsilon$ x $10^3$ |
|---|---|---|---|
| 1 | 8.8 | 0.18 | 3.7 |
| 2 | 3.2 | 0.20 | 12.5 |

**Figure 2.** (a) Distortion/interaction−activation strain model analysis; and (b) energy decomposition analysis of the cycloaddition reaction of **1** (black) and **2** (red) with $CO_2$ (transition states indicated with a dot).[13] (c) Frontier molecular orbital diagram of the most important FMO-$LUMO_{CO2}$ orbital interaction with the calculated energy gaps, orbital overlaps, and the $S^2/\Delta\varepsilon$ terms, at consistent geometries with a N···C bond length of 2.14 Å. Computed at SMD(toluene)-M06-2X-D3/def2-TZVP using autoDIAS[14] for (a) and M06-2X-D3/TZ2P//SMD(toluene)-M06-2X-D3/def2-TZVP using PyFrag[15] for (b,c).

In conclusion, we have investigated the Lewis base, nucleophile, $F^-$ catalyzed 1,3-dipolar cycloaddition between $CO_2$ and nitrilimine. In contrast to the previous proposed mechanism,[3] we find that the reaction actually proceeds via the addition of the Lewis base $F^-$ to the dipole (i.e., nitrilimine), thereby activating the dipole, which rapidly engages in nucleophilic attack and overall cycloaddition with $CO_2$ (Scheme 3). Our distortion/interaction−activation strain analysis revealed that the mechanism behind the Lewis base catalysis was driven by the more stabilizing interaction energy between the reactants. This could be traced back to the

**Scheme 3. Novel Mechanism Emerging from Our Study for the Lewis Base $F^-$ Catalyzed 1,3-Dipolar Cycloaddition of $CO_2$ to Nitrilimines, Where $F^-$ Activates the Dipole, Instead of the Dipolarophile**

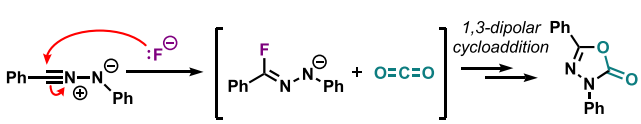



https://dx.doi.org/10.1021/acs.joc.0c02963
J. Org. Chem. 2021, 86, 4320−4325

stronger normal electron demand (NED) orbital interactions, as a result of the higher-lying donor orbitals of **2** (i.e., nitrilimine−$F^-$ species). This leads to smaller NED energy gaps and, thus, more stabilizing orbital interactions with the LUMO of $CO_2$. $F^-$ destabilizes all FMOs of **2** by (i) the presence of a negative potential of the anion and (ii) the Pauli repulsion between the filled FMOs of the nitrilimine and $F^-$. In all, this showcases the potential of Lewis base catalyzed small molecule activation, in which one can tune the reactivity of the reactants by the Lewis base.

## ■ METHODS

**Computational Details.** Conformer searches were performed using Grimme's CREST 2.7.1[16] using default settings and toluene as solvent. DFT calculations were performed using Gaussian 09 Rev. D.01[17] employing the M06-2X density functional[18] in combination with the def2-TZVP[19] basis set. Solvent effects were included by using the SMD model[20] as implemented in Gaussian with toluene as a solvent. Empirical dispersion was included using Grimme's D3 model[21] without additional dampening as proposed by Grimme and co-workers. Quasi-harmonic correction[22] was applied to all frequencies by raising all vibrations below 100 $cm^{-1}$ to 100 $cm^{-1}$. All computed stationary points have been verified by performing a vibrational analysis calculation, to be energy minima (no imaginary frequencies) or transition states (only one imaginary frequency). The character of the normal mode associated with the imaginary frequency of the transition state has been inspected to ensure that it is associated with the reaction of interest. The potential energy surfaces of the studied cycloaddition reactions were obtained by performing intrinsic reaction coordinate (IRC) calculations. The distortion/interaction−activation strain model (D/I-ASM)[9] was performed by the use of autoDIAS,[14] followed by an energy decomposition analysis (EDA)[11] in the gas phase, based on the solution PES, using PyFrag[15] and the Amsterdam Density Functional (ADF2018.106) software package at M06-2X-D3/TZ2P.[23] The optimized structures were illustrated using CYLview.[24]

**Distortion/Interaction−Activation Strain and Energy Decomposition Analysis.** The distortion/interaction−activation strain model[9] is a fragment-based approach in which the potential energy surface (PES) can be described with respect to, and understood in terms of the characteristics of, the reactants. It considers the rigidity of the reactants and to which extent they need to deform during the reaction plus their capability to interact with each other as the reaction proceeds. With the help of this model, we decompose the total energy, $\Delta E$, into the strain and interaction energy, $\Delta E_{strain}$ and $\Delta E_{int}$, respectively [eq 1].

$$\Delta E = \Delta E_{strain} + \Delta E_{int} \tag{1}$$

In this equation, the strain energy, $\Delta E_{strain}$, is the energy required in order to deform the reactants from their equilibrium to the geometry they adopt over the course of the reaction. On the other hand, the interaction energy, $\Delta E_{int}$, accounts for all the chemical interactions that occur between these two deformed reactants along the reaction coordinate.

The interaction energy between the deformed reactants can be further analyzed in terms of quantitative Kohn−Sham molecular orbital (KS-MO)[10] theory together with a canonical energy decomposition analysis (EDA).[11] The EDA decomposes the $\Delta E_{int}$ into the following three energy terms [eq 2]:

$$\Delta E_{int} = \Delta V_{elstat} + \Delta E_{Pauli} + \Delta E_{oi} + \Delta E_{disp} \tag{2}$$

Herein, $\Delta V_{elstat}$ is the classical electrostatic interaction between the unperturbed charge distributions of the (deformed) reactants and is usually attractive. The Pauli repulsion, $\Delta E_{Pauli}$, includes the destabilizing interaction between the fully occupied orbitals of both fragments due to the Pauli principle. The orbital interaction energy, $\Delta E_{oi}$, accounts for, among others, charge transfer between the fragments, such as HOMO−LUMO interactions. Finally, the $\Delta E_{disp}$ term accounts for the interactions coming from disperion forces. In the herein presented distortion/interaction−activation strain and accompanied energy decomposition diagrams, the energy terms are projected onto the forming bond (N···C) distance. This critical reaction coordinate undergoes a well-defined change during the reaction from the reactant complex via the transition state to the product.[12]

**Voronoi Deformation Density.** The atomic charge distribution was analyzed by using the Voronoi Deformation Density (VDD) method.[25] The VDD method partitions the space into so-called Voronoi cells, which are nonoverlapping regions of space that are closer to nucleus A than to any other nucleus. The charge distribution is determined by taking a fictitious promolecule as reference point, in which the electron density is simply the superposition of the atomic densities. The change in density in the Voronoi cell when going from this promolecule to the final molecular density of the interacting system is associated with the VDD atomic charge Q. The VDD atomic charge $Q_A$ of atom A is calculated according to eq 3.

$$Q_A^{VDD} = -\int_{\text{Voronoi cell of A}} [\rho(r) - \rho_{promolecule}(r)]\, dr \tag{3}$$

So, instead of computing the amount of charge contained in an atomic volume, we compute the flow of charge from one atom to the other upon formation of the molecule. The physical interpretation is therefore straightforward. A positive atomic charge $Q_A$ corresponds to the loss of electrons, whereas a negative atomic charge $Q_A$ is associated with the gain of electrons in the Voronoi cell of atom A.

## ■ ASSOCIATED CONTENT

### Supporting Information

The Supporting Information is available free of charge at https://pubs.acs.org/doi/10.1021/acs.joc.0c02963.

Additional computational results; and Cartesian coordinates, energies, and number of imaginary frequencies of all stationary points (PDF)

## ■ AUTHOR INFORMATION


### Corresponding Author

**Trevor A. Hamlin** − *Department of Theoretical Chemistry, Amsterdam Institute of Molecular and Life Sciences (AIMSS), Amsterdam Center for Multiscale Modeling (ACMM), Vrije Universiteit Amsterdam, 1081 HV Amsterdam, The Netherlands;* orcid.org/0000-0002-5128-1004; Email: t.a.hamlin@vu.nl

### Authors

**Dennis Svatunek** − *Department of Theoretical Chemistry, Amsterdam Institute of Molecular and Life Sciences (AIMSS), Amsterdam Center for Multiscale Modeling (ACMM), Vrije Universiteit Amsterdam, 1081 HV Amsterdam, The Netherlands; Institute of Applied Synthetic Chemistry, TU Wien (Vienna University of Technology), A-1060 Vienna, Austria; Department of Chemistry and Biochemistry, University of California, Los Angeles, California 90095 Los Angeles, United States*

**Thomas Hansen** − *Department of Theoretical Chemistry, Amsterdam Institute of Molecular and Life Sciences (AIMSS), Amsterdam Center for Multiscale Modeling (ACMM), Vrije Universiteit Amsterdam, 1081 HV Amsterdam, The Netherlands; Leiden Institute of Chemistry, Leiden University, 2333 CC Leiden, The Netherlands;* orcid.org/0000-0002-6291-1569

**Kendall N. Houk** − *Department of Chemistry and Biochemistry, University of California, Los Angeles,*




https://dx.doi.org/10.1021/acs.joc.0c02963
J. Org. Chem. 2021, 86, 4320−4325

*California 90095 Los Angeles, United States;* orcid.org/0000-0002-8387-5261

Complete contact information is available at: https://pubs.acs.org/10.1021/acs.joc.0c02963

### Author Contributions

[+]D.S. and T.H. contributed equally to this work.

### Notes

The authors declare no competing financial interest.

## ■ ACKNOWLEDGMENTS

D.S. is grateful to the Christiana Hörbiger Award (TU Wien) and the "Hochschuljubiläumsstiftung der Stadt Wien" (H-331849/2018) for financial support. K.N.H. is grateful to the National Science Foundation of the US for financial support of this research (CHE-1764328). Quantum chemical calculations were performed on the Vienna Scientific Cluster (Austria), the Hoffman2 Cluster (UCLA Institute for Digital Research and Education), and the Cartesius supercomputer (SURFsara, Amsterdam). The authors also acknowledge Pascal Vermeeren of the Vrije Universiteit Amsterdam for fruitful discussions.

## ■ REFERENCES

(1) (a) Milani, B.; Licini, G.; Clot, E.; Albrecht, M. Small Molecule Activation. *Dalton Trans.* **2016**, *45*, 14419−14420. (b) Zhang, W.; Lai, W.; Cao, R. Energy-Related Small Molecule Activation Reactions: Oxygen Reduction and Hydrogen and Oxygen Evolution Reactions Catalyzed by Porphyrin- and Corrole-Based Systems. *Chem. Rev.* **2017**, *117*, 3717−3797. (c) Gómez, J. E.; Kleij, A. W. Catalytic Nonreductive Valorization of Carbon Dioxide into Fine Chemicals. In *Adv. Organomet. Chem.*; Pérez, P. J., Ed.; Academic Press: 2019; Vol. *71*, pp 175−226. (d) Chen, L.; Chen, G.; Leung, C.-F.; Cometto, C.; Robert, M.; Lau, T.-C. Molecular Quaterpyridine-Based Metal Complexes for Small Molecule Activation: Water Splitting and $CO_2$ Reduction. *Chem. Soc. Rev.* **2020**, *49*, 7271−7283.

(2) (a) Liu, Q.; Wu, L.; Jackstell, R.; Beller, M. Using Carbon Dioxide as a Building Block in Organic Synthesis. *Nat. Commun.* **2015**, *6*, 5933. (b) Vogt, C.; Monai, M.; Sterk, E. B.; Palle, J.; Melcherts, A. E. M.; Zijlstra, B.; Groeneveld, E.; Berben, P. H.; Boereboom, J. M.; Hensen, E. J. M.; Meirer, F.; Filot, I. A. W.; Weckhuysen, B. M. Understanding Carbon Dioxide Activation and Carbon-Carbon Coupling over Nickel. *Nat. Commun.* **2019**, *10*, 5330. (c) Schilling, W.; Das, S. Transition Metal-Free Synthesis of Carbamates Using $CO_2$ as the Carbon Source. *ChemSusChem* **2020**, *13*, 6246−6258.

(3) Guo, C.-X.; Zhang, W.-Z.; Zhang, N.; Lu, X.-B. 1,3-Dipolar Cycloaddition of Nitrile Imine with Carbon Dioxide: Access to 1,3,4-Oxadiazole-2(3*H*)-ones. *J. Org. Chem.* **2017**, *82*, 7637.

(4) (a) Zhang, X.; Gross, U.; Seppelt, K. Fluorocarbonate, $[FCO_2]^-$: Preparation and Structure. *Angew. Chem., Int. Ed. Engl.* **1995**, *34*, 1858−1860. (b) Arnold, D. W.; Bradforth, S. E.; Kim, E. H.; Neumark, D. M. Study of halogen-carbon dioxide clusters and the fluoroformyloxyl radical by photodetachment of $X^-(CO_2)$ (X= I, Cl, Br) and $FCO_2^-$. *J. Chem. Phys.* **1995**, *102*, 3493.

(5) (a) Ukai, K.; Aoki, M.; Takaya, J.; Iwasawa, N. Rhodium(I)-Catalyzed Carboxylation of Aryl- and Alkenylboronic Esters with $CO_2$. *J. Am. Chem. Soc.* **2006**, *128*, 8706. (b) Li, S.; Ma, S. Quadri-Synergetic Effect for Highly Effective Carbon Dioxide Fixation and Its Application to Indoloquinolinone. *Adv. Synth. Catal.* **2012**, *354*, 2387−2394. (c) Takaya, J.; Tadami, S.; Ukai, K.; Iwasawa, N. Copper (I)-catalyzed carboxylation of aryl-and alkenylboronic esters. *Org. Lett.* **2008**, *10*, 2697−2700.

(6) Denmark, S. E.; Beutner, G. L. Lewis Base Catalysis in Organic Synthesis. *Angew. Chem., Int. Ed.* **2008**, *47*, 1560−1638.

(7) Murillo, F.; Barroso, J.; de los Santos, M. G.; Ávila, G.; Pan, S.; Fernández-Herrera, M. A.; Merino, G. Revisiting the Formation Mechanism of 1,3,4-Oxadiazole-2(3*H*)-ones from Hydrazonyl Chloride and Carbon Dioxide. *J. Org. Chem.* **2018**, *83*, 13045−13050.

(8) (a) Wang, X. S.; Lee, Y. J.; Liu, W. R. The nitrilimine-alkene cycloaddition is an ultra rapid click reaction. *Chem. Commun.* **2014**, *50*, 3176−3179. (b) Molteni, G.; Ponti, A. The Nitrilimine-Alkene Cycloaddition Regioselectivity Rationalized by Density Functional Theory Reactivity Indices. *Molecules* **2017**, *22*, 202. (c) Shawali, A. S. Chemoselectivity in 1,3-dipolar cycloaddition reactions of nitrilimines with multifunctionalized dipolarophiles. *Curr. Org. Chem.* **2014**, *18*, 598−614.

(9) (a) Bickelhaupt, F. M.; Houk, K. N. Analyzing Reaction Rates with the Distortion/Interaction-Activation Strain Model. *Angew. Chem., Int. Ed.* **2017**, *56*, 10070−10086; *Angew. Chem.* **2017**, *129*, 10204−10221. (b) Vermeeren, P.; van der Lubbe, S. C. C.; Fonseca Guerra, C.; Bickelhaupt, F. M.; Hamlin, T. A. Understanding Chemical Reactivity Using the Activation Strain Model. *Nat. Protoc.* **2020**, *15*, 649−667. (c) Fernández, I.; Bickelhaupt, F. M. The activation strain model and molecular orbital theory: understanding and designing chemical reactions. *Chem. Soc. Rev.* **2014**, *43*, 4953−4967.

(10) Bickelhaupt, F. M.; Baerends, E. J. Kohn-Sham Density Functional Theory: Predicting and Understanding Chemistry. In *Reviews in Computational Chemistry*; Lipkowitz, K. B., Boyd, D. B., Eds.; Wiley-VCH: New York, 2000; Vol. *15*, pp 1−86.

(11) (a) van Meer, R.; Gritsenko, O. V.; Baerends, E. J. Physical Meaning of Virtual Kohn-Sham Orbitals and Orbital Energies: An Ideal Basis for the Description of Molecular Excitations. *J. Chem. Theory Comput.* **2014**, *10*, 4432−4441.

(12) (a) Yu, S.; Vermeeren, P.; van Dommelen, K.; Bickelhaupt, F. M.; Hamlin, T. A. Understanding the 1,3-Dipolar Cycloadditions of Allenes. *Chem. - Eur. J.* **2020**, *26*, 11529−11539. (b) Hamlin, T. A.; Levandowski, B. J.; Narsaria, A. K.; Houk, K. N.; Bickelhaupt, F. M. Bickelhaupt. Structural Distortion of Cycloalkynes Influences Cycloaddition Rates by both Strain and Interaction Energies. *Chem. - Eur. J.* **2019**, *25*, 6342−6348. (c) Hamlin, T. A.; Svatunek, D.; Yu, S.; Ridder, L.; Infante, I.; Visscher, L.; Bickelhaupt, F. M. Elucidating the Trends in Reactivity of Aza-1,3-Dipolar Cycloadditions. *Eur. J. Org. Chem.* **2019**, *2019*, 378−386.

(13) Differences in the dispersion curves were neglectable and were omitted for clarity.

(14) Svatunek, D.; Houk, K. N. autoDIAS: a python tool for an automated distortion/interaction activation strain analysis. *J. Comput. Chem.* **2019**, *40*, 2509.

(15) Sun, X.; Soini, T. M.; Poater, J.; Hamlin, T. A.; Bickelhaupt, F. M. PyFrag 2019—Automating the exploration and analysis of reaction mechanisms. *J. Comput. Chem.* **2019**, *40*, 2227.

(16) (a) Pracht, P.; Bohle, F.; Grimme, S. Automated exploration of the low-energy chemical space with fast quantum chemical methods. *Phys. Chem. Chem. Phys.* **2020**, *22*, 7169−7192. (b) Grimme, S.; Bannwarth, C.; Dohm, S.; Hansen, A.; Pisarek, J.; Pracht, P.; Neese, F. Fully Automated Quantum-Chemistry-Based Computation of Spin-Spin-Coupled Nuclear Magnetic Resonance Spectra. *Angew. Chem., Int. Ed.* **2017**, *56*, 14763−14769.

(17) Frisch, M. J.; Trucks, G. W.; Schlegel, H. B.; Scuseria, G. E.; Robb, M. A.; Cheeseman, J. R.; Scalmani, G.; Barone, V.; Mennucci, B.; Petersson, G. A.; Nakatsuji, H.; Caricato, M.; Li, X.; Hratchian, H. P.; Izmaylov, A. F.; Bloino, J.; Zheng, G.; Sonnenberg, J. L.; Hada, M.; Ehara, M. et al. *Gaussian 09*, rev. D.01; Gaussian Inc.: Wallingford, CT, 2009.

(18) Zhao, Y.; Truhlar, D. G. The M06 suite of density functionals for main group thermochemistry, thermochemical kinetics, noncovalent interactions, excited states, and transition elements: two new functionals and systematic testing of four M06-class functionals and 12 other functionals. *Theor. Chem. Acc.* **2008**, *120*, 215.

(19) Weigend, F.; Ahlrichs, R. Balanced basis sets of split valence, triple zeta valence and quadruple zeta valence quality for H to Rn: Design and assessment of accuracy. *Phys. Chem. Chem. Phys.* **2005**, *7*, 3297−3305.

(20) Marenich, A. V.; Cramer, C. J.; Truhlar, D. G. Generalized born solvation model SM12. *J. Phys. Chem. B* **2009**, *113*, 6378.
(21) Goerigk, L.; Hansen, A.; Bauer, C.; Ehrlich, S.; Najibi, A.; Grimme, S. A look at the density functional theory zoo with the advanced GMTKN55 database for general main group thermochemistry, kinetics and noncovalent interactions. *Phys. Chem. Chem. Phys.* **2017**, *19*, 32184.
(22) Ribeiro, R. F.; Marenich, A. V.; Cramer, C. J.; Truhlar, D. G. Use of solution-phase vibrational frequencies in continuum models for the free energy of solvation. *J. Phys. Chem. B* **2011**, *115*, 14556.
(23) te Velde, G.; Bickelhaupt, F. M.; Baerends, E. J.; Fonseca Guerra, C.; van Gisbergen, S. J. A.; Snijders, J. G.; Ziegler, T. Chemistry with ADF. *J. Comput. Chem.* **2001**, *22*, 931.
(24) Legault, C. Y. *CYLview*, 1.0b; Université de Sherbrooke: Canada, Sherbrooke, QC, 2009, www.cylview.org.
(25) Fonseca Guerra, C.; Handgraaf, J. W.; Baerends, E. J.; Bickelhaupt, F. M. Voronoi deformation density (VDD) charges: Assessment of the Mulliken, Bader, Hirshfeld, Weinhold, and VDD methods for charge analysis? *J. Comput. Chem.* **2004**, *25*, 189−210.



https://dx.doi.org/10.1021/acs.joc.0c02963
*J. Org. Chem.* 2021, 86, 4320−4325